

**Electronic Supplementary information**

**Mesoporous MnCo<sub>2</sub>S<sub>4</sub> Nanosheet Arrays as Efficient  
Catalyst for Li-O<sub>2</sub> Battery**

*Zoya Sadighi<sup>a</sup>, Jiapeng Liu<sup>a</sup>, Francesco Ciucci<sup>a,b</sup>, Jang-Kyo Kim<sup>\*a</sup>*

<sup>a</sup> Department of Mechanical and Aerospace Engineering, The Hong Kong University of Science and Technology, Clear Water Bay, Hong Kong

<sup>b</sup> Department of Chemical and Biological Engineering, The Hong Kong University of Science and Technology, Clear Water Bay, Hong Kong

\* Corresponding author. J.-K. Kim. E-mail address: mejkkim@ust.hk. Tel: +852 2358 7207, Fax: +852 2358 1543.

## Preparation of Electrode Materials

MnCo<sub>2</sub>S<sub>4</sub> nanosheets were deposited on a carbon paper (MCS/CP) by a facile, quick electrodeposition process requiring low energy, followed by low temperature vulcanization. In a typical process, 5 mM (0.3 mmole) cobalt (II) sulfate heptahydrate (CoSO<sub>4</sub>·7H<sub>2</sub>O<sub>4</sub>, Aldrich 99%), 10 mM (0.6 mmole) manganese (II) sulfate monohydrate (MnSO<sub>4</sub>·H<sub>2</sub>O, UNI-CHEM 99%) and 0.5 M (30 mmole) thiourea (CH<sub>4</sub>N<sub>2</sub>S, Aldrich 99%) were dissolved in 60 ml deionized (DI) water under magnetic stirring for 30 min. The CP (TGP-H-060, 0.19 mm thickness, Toray Co.) was cut into disks of 14 mm in diameter and was washed several times with DI water and acetone under sonication. The electrodeposition was carried out in a three electrode cell configuration using the CP as working electrode, Pt as counter electrode and Ag/AgCl as reference electrode at a scan rate of 5 mV s<sup>-1</sup> for 15 cycles in a voltage range from -1.2 to 0.2 V vs Ag/AgCl. One side of CP disks was covered by a conductive copper tape while nanosheets (NSs) were grown on the other side. After removing the copper tape upon completion of electrodeposition, the loose particles on the deposited thin layer was rinsed using DI water, followed by drying in a vacuum oven at 80 °C overnight. After covering the portion of no deposit using an insulating tape, the CP was immersed in 30 ml 0.4 M CH<sub>4</sub>N<sub>2</sub>S solution, which was hydrothermally treated in a Teflon-lined stainless steel autoclave at 180 °C for 10 h. After cooling to ambient temperature, the sulfurized MCS NSs on CP were washed with DI water and dried under vacuum at 80 °C overnight. MnCo<sub>2</sub>O<sub>4</sub> NS arrays were also grown on carbon paper (MCO/CP) using the same electrodeposition method, but with acetate precursors (Co(C<sub>2</sub>H<sub>3</sub>O<sub>2</sub>)<sub>2</sub>·4H<sub>2</sub>O and Mn(C<sub>2</sub>H<sub>3</sub>O<sub>2</sub>)<sub>2</sub>·4H<sub>2</sub>O, UNI-CHEM 99%) and urea of the same molar ratios as stated above.

## Characterization

Field emission scanning electron microscopy (FESEM, JEOL-6700F) and transmission electron microscopy (TEM, JEOL 2010) were used to examine the micro- and nanostructures of NSs. The elemental maps of NSs were obtained by energy dispersive X-ray spectroscopy (EDX). The crystallinity of NSs was examined by X-ray diffraction (XRD) (Philips PW1830) with Cu K $\alpha$  radiation in the  $2\theta$  range of 10-80° at room temperature. A slow scan rate of 0.02° s<sup>-1</sup> was used in the thin film mode for XRD. Raman spectroscopy (Renishaw PLC) was conducted at a laser excitation wavelength of 514 nm. X-ray photoelectron spectroscopy (XPS, PHI5600, Physical Electronics) was performed to analyze the surface chemistries in the depth of  $\leq 5$  nm from surface using Al K $\alpha$  X-ray spectrometer at 14 kV and the spectra were calibrated with C 1s (285.0 eV). The specific surface area was measured using the nitrogen adsorption/desorption isotherm curves obtained on a Coulter SA 3100 surface area instrument based on the Brunauer-Emmett-Teller (BET) method, and the pore volume was calculated using the adsorption Barrett–Joyner–Halenda (BJH) method. The electrical conductivities were measured using a four-probe resistivity/Hall system (HK5500PC, Bio-Rad).

## Electrochemical Measurements

A custom-built device was used to fabricate the LOB cells as in our previous studies (Fig. S1).<sup>S1-</sup>  
<sup>S3</sup> The electrodes made of NSs on CP (MCS/CP and MCO/CP) were applied as freestanding and binder-free cathodes. The LOB cells were constructed in an Ar-filled glove box with lithium foil as anode, glass fiber separator (Whatman, GF/D), electrolyte prepared from 0.5 M LiTFSI in TEGDME solution and the aforementioned cathodes. Because the CP was used as both current collector and gas diffusion layer (GDL), the mass loading of NSs was calculated from the mass

difference of CP before and after NS growth, which was about  $0.6 \text{ mg cm}^{-2}$ . The current densities and specific capacities were determined based on the NS mass content. Before the electrochemical tests, the cells were purged with 99.5% pure  $\text{O}_2$  for 0.5 h and kept for 3 h before reaching a stable open-circuit voltage. The discharge/charge curves were determined in the potential range of 2.0-4.5 V on a LAND 2001 CT battery tester. The cyclic tests were conducted at a current density of  $200 \text{ mA g}^{-1}$  and an upper-limit capacity of  $500 \text{ mAh g}^{-1}$ . The electrochemical impedance spectroscopy (EIS) analysis was performed at different stages of discharge/charge process in the frequency range between 10 mHz and 100 kHz and at a constant perturbation amplitude of 5 mV on a CHI660c electrochemical workstation. The cyclic voltammetry (CV) tests were conducted at scan rates varying from  $0.1$  to  $0.3 \text{ mV s}^{-1}$  in the potential range of 2-4.5 V.

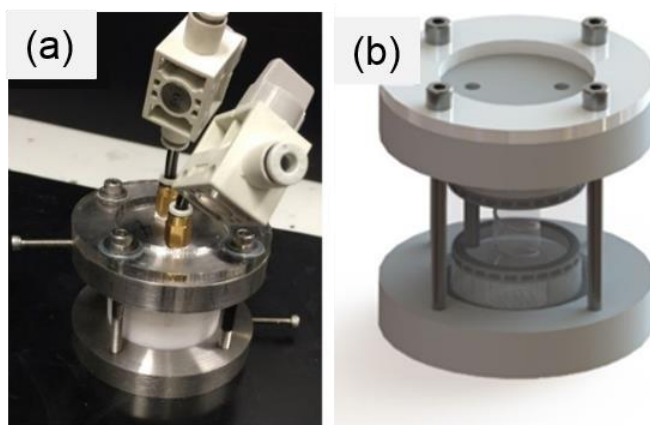


**Figure S1.** Photographs of (a) Li-O<sub>2</sub> battery testing device and (b) cell.<sup>S1-S3</sup>

### Theoretical calculations

The density functional theory (DFT) calculations based on the first principles were used to estimate the binding energies of discharge products with both MCS and MCO NSs to verify the relative capacities of the batteries containing different electrodes. All spin-polarized calculations were performed using Vienna *ab initio* simulation package (VASP)<sup>S4</sup> with plane wave basis set and a

projector-augmented wave (PAW) approach.<sup>S5</sup> A kinetic energy cutoff of 520 eV was selected. The exchange-correlation was described using the Perdew-Burk-Ernzerhof (PBE) functional<sup>S6</sup> under the generalized gradient approximation (GGA) scheme. All the atoms were allowed to relax using the conjugated gradient method until a convergence criterion of  $10^{-5}$  eV for energy and 0.02 eV Å<sup>-1</sup> for force. Initially, the Mn<sub>x</sub>Co<sub>3-x</sub>S<sub>4</sub> ( $x = 0.25, 0.5, 0.75, 1$ ) compounds were considered in which the Mn<sup>2+</sup> ions substituted the Co<sup>2+</sup> sites. The DFT calculations revealed negative formation energies for all stoichiometries with relatively small absolute values, indicating the tendency of ternary sulfide to decompose and form binary sulfides, e.g. Co<sub>3</sub>S<sub>4</sub>, Co<sub>9</sub>S<sub>8</sub> and MnS<sub>2</sub>, at a positive energy above hull. However, previous experimental studies reported the synthesis of Mn<sub>x</sub>Co<sub>3-x</sub>S<sub>4</sub> compounds.<sup>S7-10</sup> The discrepancy arose from the ideal conditions, such as T= 0 K and P= 0 atm, considered prior to the DFT calculations. Similarly, Mn<sub>x</sub>Co<sub>3-x</sub>O<sub>4</sub> was not stable according to the computation results, although it was synthesized previously.<sup>S11-17</sup> In this regard, the calculations were continued with a given stoichiometry of MnCo<sub>2</sub>S<sub>4</sub> (MCS). The bulk MCS was simulated with an initial cubic structure of space group Fd $\bar{3}$ m (Fig. S11a). The Brillouin-zone was sampled with a Gamma centered 3×3×3 *k*-point mesh. A structural search was conducted using the enumlib package<sup>S18</sup> wrapped in the pymatgen code<sup>S19</sup> to account for fractional stoichiometry. The (110) plane of MCS was chosen due to its lowest surface energy, in agreement with the HRTEM image (Fig. 2j). To study the interaction between the catalyst and Li<sub>2</sub>O<sub>2</sub> or LiO<sub>2</sub>, a four-layer MCS surface slab was modeled with a vacuum space of 12 Å along the *c*-direction and the interactions between different slabs were cancelled. The atoms in the bottom two layers were fixed to simulate the bulk properties while the top two layers were allowed to relax until saturation. Equation (S1) was used to measure the adsorption energy of Li<sub>2</sub>O<sub>2</sub> or LiO<sub>2</sub> on the surface:<sup>S20</sup>

$$E_{\text{ads}} = E_{\text{sys}} - nE_{\text{Li}} - E_{\text{O}_2} \quad (\text{S1})$$

where  $E_{\text{sys}}$  is the total energy of  $\text{Li}_2\text{O}_2$  or  $\text{LiO}_2$  adsorbed on the surface, and  $E_{\text{Li}}$  corresponds to the energy of Li in the bulk metal state,  $E_{\text{O}_2}$  is the energy of molecule in a triple state to eliminate the over-binding problem, and  $n$  is the number of Li atoms in  $\text{Li}_2\text{O}_2$  or  $\text{LiO}_2$ , either 2 or 1. The charge difference was defined by Equation (S2):<sup>S20</sup>

$$\rho_{\text{diff}} = \rho_{\text{sys}} - \rho_{\text{Li-O}} - \rho_{\text{sub}} \quad (\text{S2})$$

where  $\rho_{\text{sys}}$  is the charge density of the system with  $\text{Li}_2\text{O}_2$  or  $\text{LiO}_2$  adsorbed on the surface,  $\rho_{\text{Li-O}}$  is the charge density of either  $\text{Li}_2\text{O}_2$  or  $\text{LiO}_2$ , and  $\rho_{\text{sub}}$  is the charge density of the substrate, i.e., the slab model considered here.<sup>S1,S3,S9</sup> Finally, for decomposition of  $\text{Li}_2\text{O}_2$  during OER, the reaction free energies were calculated using Equation (S3):

$$\Delta G_n = E_{\text{tot}(n)} - E_{\text{tot}(n-1)} - E_{\text{ori}} \quad (\text{S3})$$

Where  $E_{\text{tot}(n)}$ ,  $E_{\text{tot}(n-1)}$  and  $E_{\text{ori}}$  represent the total binding energy of the adsorption configuration at the (n)<sup>th</sup> step, at the (n-1)<sup>th</sup> step, and the original energy of the adsorbed species (Li or  $\text{O}_2$ ).<sup>S20</sup> The simulations were repeated for MCO in the same manner.

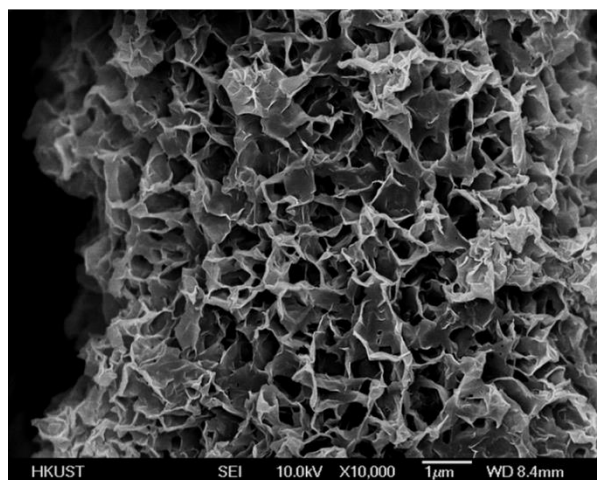


**Figure S2.** FESEM image of Mn-Co-sulfate NSs.

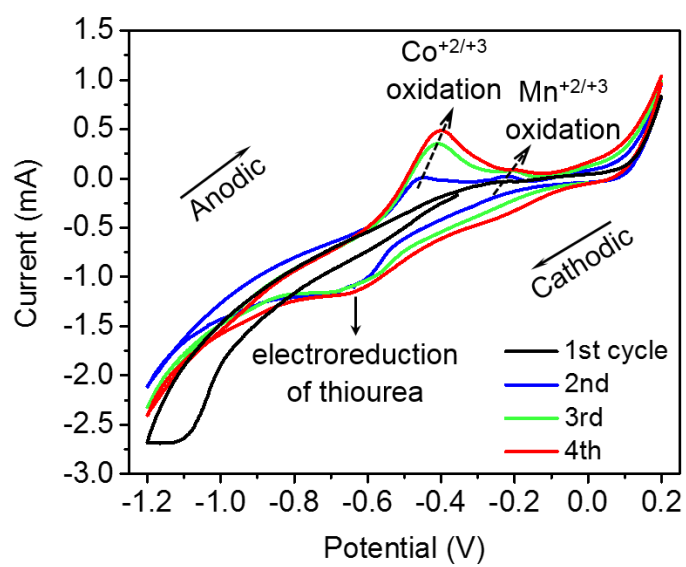


**Figure S3.** CV curves of the electrodeposition of MCS NSs on CP in the first four cycles.

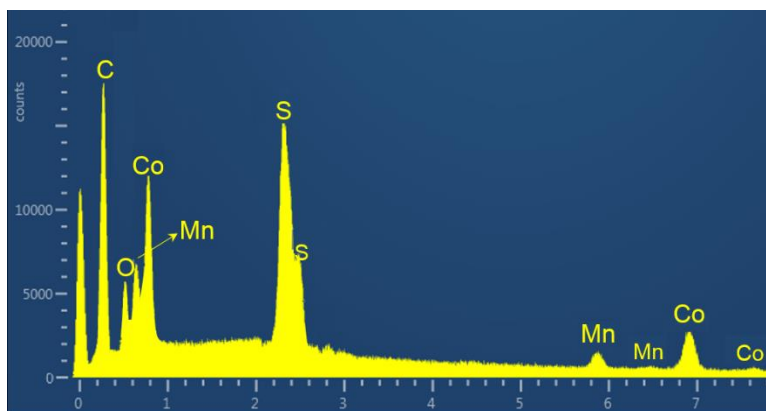


**Figure S4.** EDX spectrum of MCS/CP.

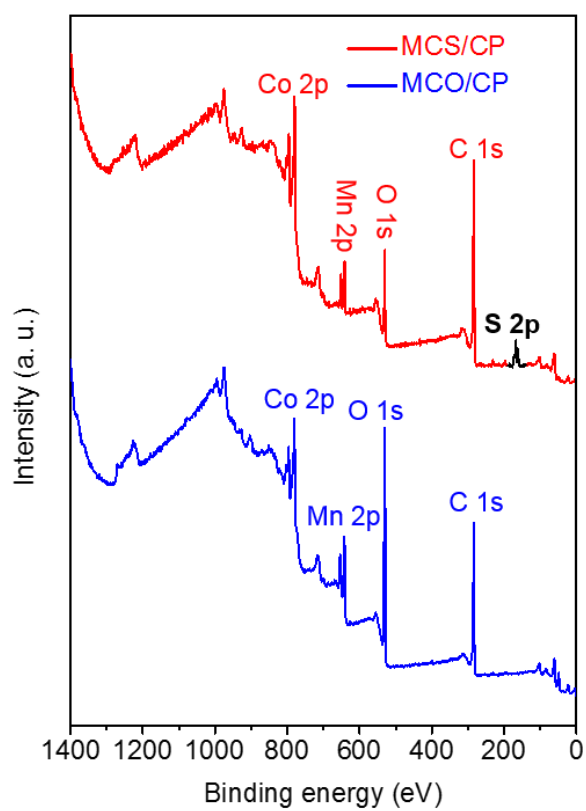


**Figure. S5.** General XPS spectra of MCS/CP and MCO/CP.

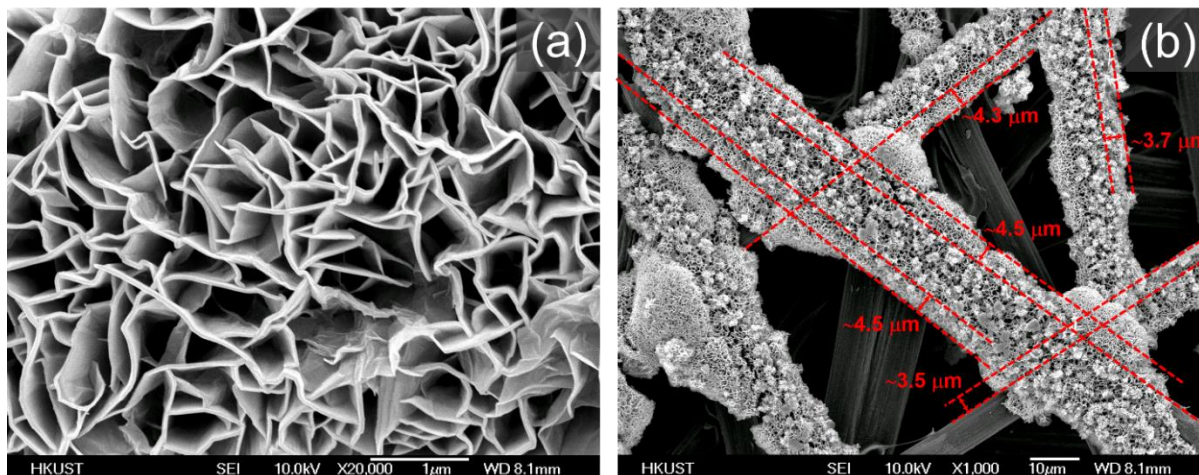


**Figure S6.** FESEM images of MCS/CP electrode. (a) MCS NSs are deposited perpendicular to the carbon fiber surface. (b) The MCS NSs coating thickness on several fibers are indicated by red dotted lines.

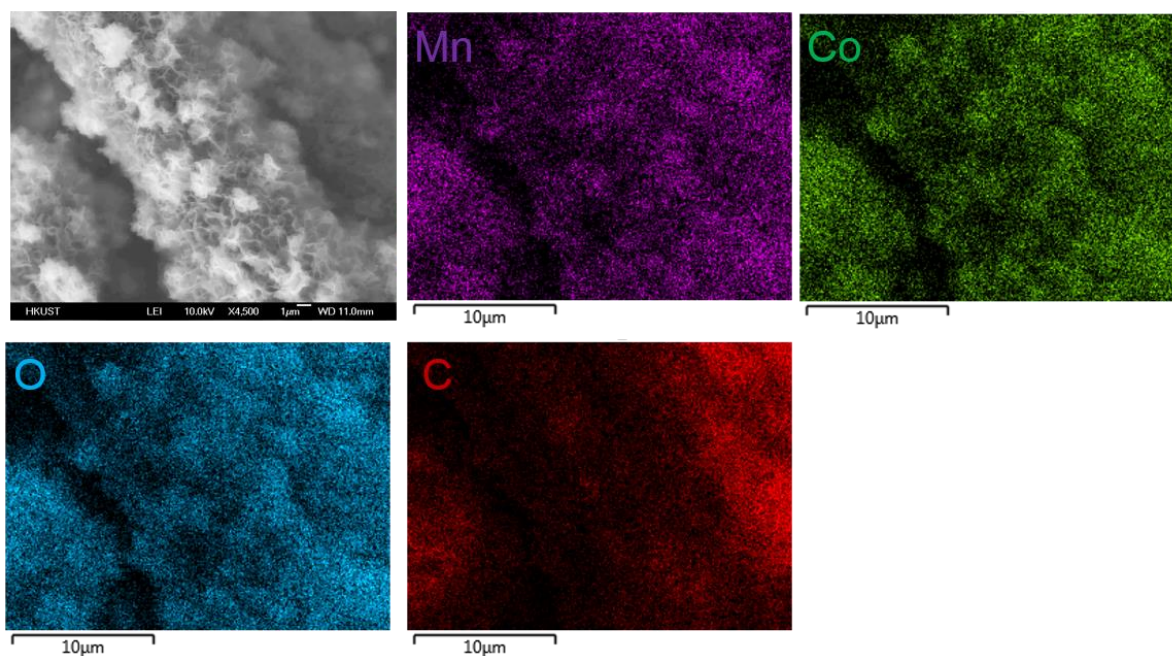


**Figure S7.** EDX elemental maps of MCO/CP.

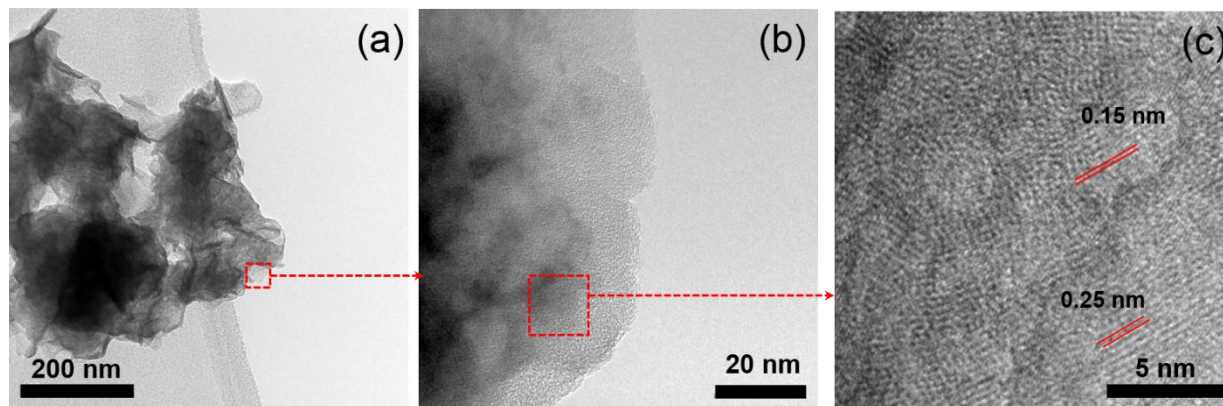


**Figure S8.** TEM and HRTEM images of electrodeposited MCO NSs on NSs.

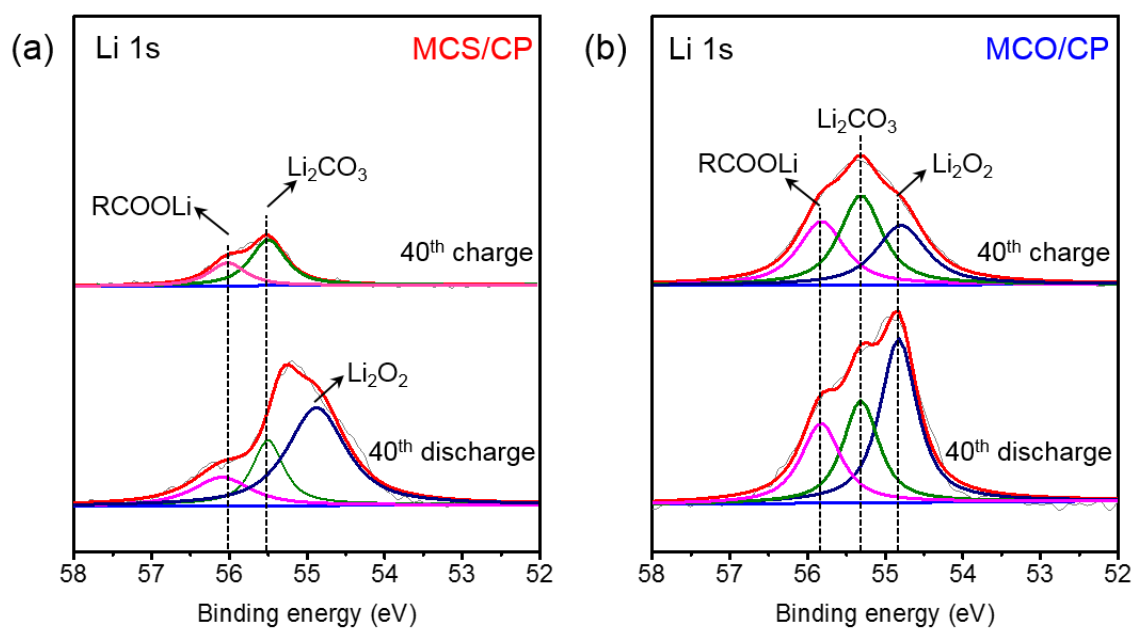


**Figure S9.** *Ex situ* XPS spectra: deconvoluted Li 1s of (a) the MCS/CP and (b) MCO/CP cathodes after the 40<sup>th</sup> discharge and charge cycles.

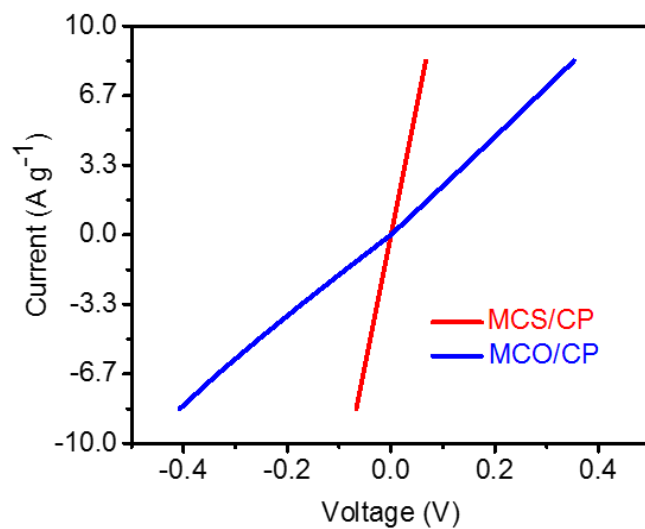


**Figure S10.** Current-voltage (I-V) graphs of MCS/CP and MCO/CP.

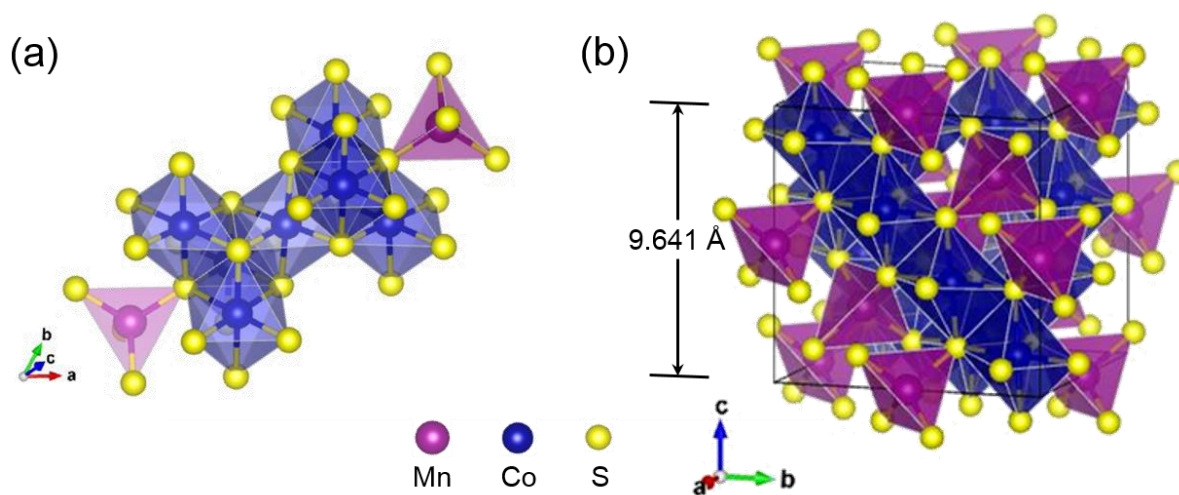


**Figure S11.** Schematics of MCS (a) primitive- and (b) super-cells.

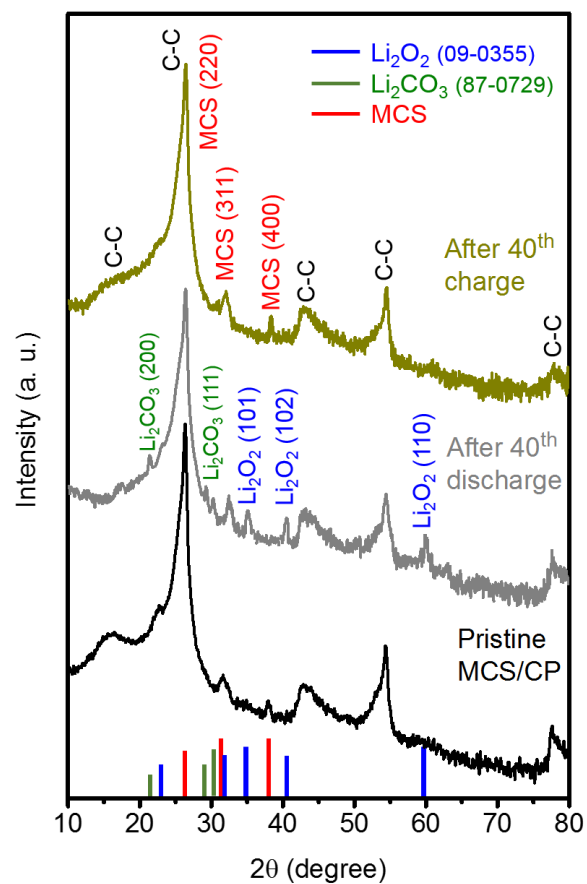


**Figure S12.** *Ex situ* XRD spectra of the MCS/CP electrode taken before and after the 40<sup>th</sup> discharge and charge at 200 mA g<sup>-1</sup> at an upper-limit capacity of 500 mAh g<sup>-1</sup>.

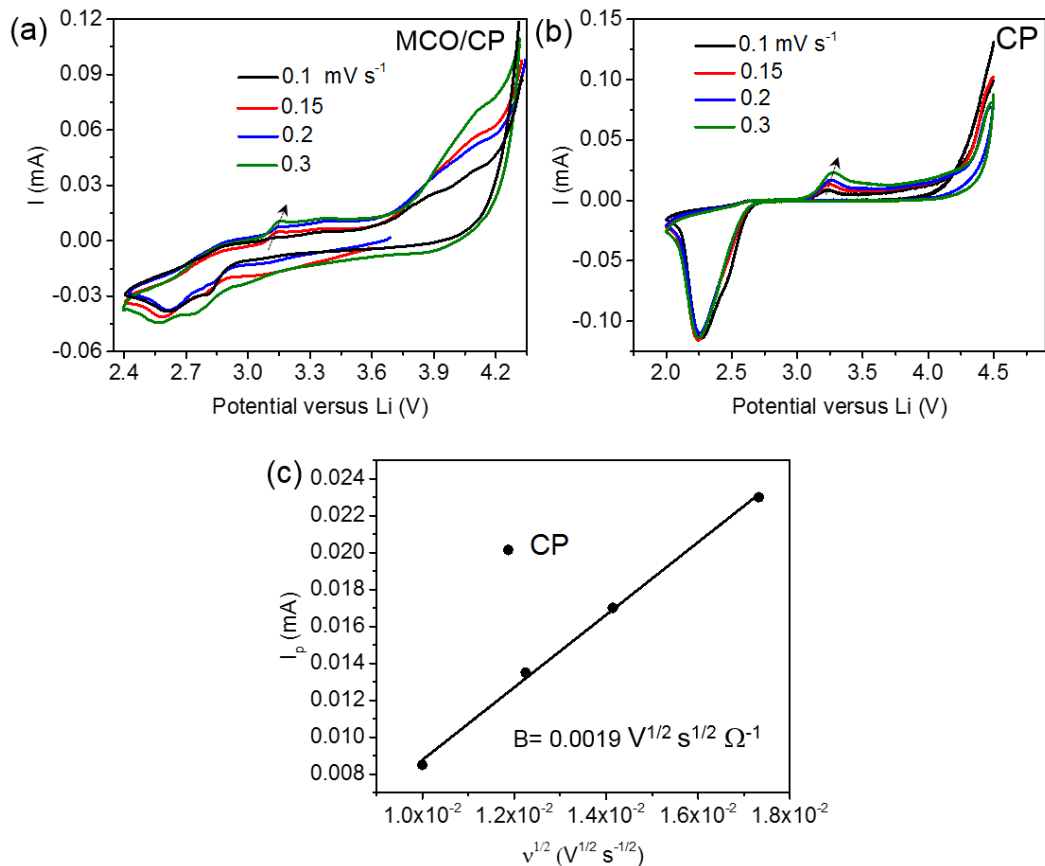


**Figure S13.** CV curves of the (a) MCO/CP and (b) CP electrodes measured at the third and following charge/discharge cycles at different rates of 0.1, 0.15, 0.2, 0.3  $\text{mV s}^{-1}$ . (c) Anodic peak current of CP electrode versus square root of scan rate,  $v^{1/2}$ .

**Table S1.** Specific surface area, pore volume, electrical conductivity and lithium diffusion coefficient of different electrodes.

Materials	BET surface area ( $\text{m}^2 \text{g}^{-1}$ )	Pore volume ( $\text{cm}^3 \text{g}^{-1}$ )	Electrical conductivity ( $\text{S cm}^{-1}$ )	lithium diffusion coefficient ( $\text{cm}^2 \text{s}^{-1}$ )
MCS/CP	65.4	0.41	5.35	$1.54 \times 10^{-12}$
MCO/CP	27.4	0.083	1.13	$6.05 \times 10^{-13}$

**Table S2.** Surface area and energy of three low-index surfaces of MCS predicted by the DFT calculations.

Surface	Surface Area ( $\text{\AA}^2$ )	Surface energy ( $\text{J m}^{-2}$ )
001	92.95	0.81
110	131.45	0.72
111	160.99	1.34

**Table S3.** Impedance parameters calculated from the equivalent circuit.

	State	MCO/CP	MCS/CP
$R_s / \Omega$	Fresh	19.4	21.5
	After 1 <sup>st</sup> discharge	26.7	23.1
	After 1 <sup>st</sup> charge	29.5	24.4
	After 40 <sup>th</sup> cycles	33.5	25.2
$R_{ct} / \Omega$	Fresh	467.3	133.4
	After 1 <sup>st</sup> discharge	815.2	385.5
	After 1 <sup>st</sup> charge	1325.3	303.2
	After 40 <sup>th</sup> cycles	2691	172.5
$CPE_{dl} / \mu\text{F}$	Fresh	11.4	14.1
	After 1 <sup>st</sup> discharge	5.3	133.6
	After 1 <sup>st</sup> charge	8.6	319.5
	After 40 <sup>th</sup> cycles	4.1	477.3
$Z_w / \Omega$	Fresh	327.7	84.1
	After 1 <sup>st</sup> discharge	791.4	644.7
	After 1 <sup>st</sup> charge	660.2	335.3
	After 40 <sup>th</sup> cycles	2983	372.4

## SI REFERENCES

- S1 J. Huang, B. Zhang, Z. Bai, R. Guo, Z.-L. Xu, Z. Sadighi, L. Qin, T.-Y. Zhang, G. Chen, B. Huang and J.-K. Kim, *Adv. Funct. Mater.*, 2016, **26**, 8290–8299.
- S2 Z. Sadighi, J. Huang, L. Qin, S. Yao, J. Cui and J.-K. Kim, *J. Power Sources*, 2017, **365**, 134–147.
- S3 J. Huang, Z. Jin, Z.-L. Xu, L. Qin, H. Huang, Z. Sadighi, S. Yao, J. Cui, B. Huang and J.-K. Kim, *Energy Storage Mater.*, 2017, **8**, 110–118.
- S4 G. Kresse and J. Furthmüller, *Comput. Mater. Sci.*, 1996, **6**, 15–50.
- S5 P. E. Blöchl, *Phys. Rev. B*, 1994, **50**, 17953.
- S6 J. P. Perdew, K. Burke and M. Ernzerhof, *Phys. Rev. Lett.*, 1996, **77**, 3865.
- S7 S. Sahoo and C. S. Rout, *Electrochim. Acta*, 2016, **220**, 57–66.
- S8 Y. M. Chen, Z. Li and X. W. D. Lou, *Angew. Chemie*, 2015, **127**, 10667–10670.
- S9 Q. Li, Z. Xing, D. Wang, X. Sun and X. Yang, *ACS Catal.*, 2016, **6**, 2797–2801.
- S10 A. M. Elshahawy, X. Li, H. Zhang, Y. Hu, K. H. Ho, C. Guan and J. Wang, *J. Mater. Chem. A*, 2017, **5**, 7494–7506.
- S11 L. Zhou, D. Zhao and X. W. Lou, *Adv. Mater.*, 2012, **24**, 745–748.
- S12 L. Wang, X. Zhao, Y. Lu, M. Xu, D. Zhang, R. S. Ruoff, K. J. Stevenson and J. B. Goodenough, *J. Electrochem. Soc.*, 2011, **158**, A1379–A1382.
- S13 L. Hu, H. Zhong, X. Zheng, Y. Huang, P. Zhang and Q. Chen, *Sci. Rep.*, 2012, **2**, 986.
- S14 L. Zou, J. Cheng, Y. Jiang, Y. Gong, B. Chi, J. Pu and L. Jian, *RSC Adv.*, 2016, **6**, 31248–31255.
- S15 X. Ge, Y. Liu, F. W. T. Goh, T. S. A. Hor, Y. Zong, P. Xiao, Z. Zhang, S. H. Lim, B. Li, X. Wang and others, *ACS Appl. Mater. Interfaces*, 2014, **6**, 12684–12691.
- S16 S. Ma, L. Sun, L. Cong, X. Gao, C. Yao, X. Guo, L. Tai, P. Mei, Y. Zeng, H. Xie and others, *J. Phys. Chem. C*, 2013, **117**, 25890–25897.
- S17 T. Y. Ma, Y. Zheng, S. Dai, M. Jaroniec and S. Z. Qiao, *J. Mater. Chem. A*, 2014, **2**, 8676–8682.
- S18 G. L. W. Hart, L. J. Nelson and R. W. Forcade, *Comput. Mater. Sci.*, 2012, **59**, 101–107.

- S19 S. P. Ong, W. D. Richards, A. Jain, G. Hautier, M. Kocher, S. Cholia, D. Gunter, V. L. Chevrier, K. A. Persson and G. Ceder, *Comput. Mater. Sci.*, 2013, **68**, 314–319.
- S20 X. Li, Z. Li, X. Yang, L. Jia, Y. Q. Fu, B. Chi, J. Pu and J. Li, *J. Mater. Chem. A*, 2017, **5**, 3320–3329.